RSC Advances

ROYAL SOCIETY OF CHEMISTRY

www.rsc.org/advances

Journal Name

RSCPublishing

ARTICLE

Quaternary semiconductor Cu_2ZnSnS_4 loaded with MoS_2 as co-catalyst for enhanced photo-catalytic activity

Cite this: DOI: 10.1039/x0xx00000x

Received ooth January 2012,
Accepted ooth January 2012

DOI: 10.1039/x0xx00000x

www.rsc.org/

Gaurangi Gogoi[a], Sonia Arora[a], Natarajan Vinothkumar[b] , Mahuya De[b] and Mohammad Qureshi*[a]

Quaternary Cu_2ZnSnS_4 (CZTS) loaded with 1 %MoS_2 shows an excellent photo-catalytic activity for water oxidation leading to efficient H2 generation (AQY 22.67%) as well as in degrading organic pollutant. The photo catalysts were characterized by powder X-ray diffraction, Field Emission Scanning Electron Microscopy, Transmission Electron Microscopy, UV-Vis absorbance and fluorescence spectroscopy. Taking Rhodamine B as a model system, the apparent rate constant for CZTS-MoS_2 (i.e. k_{app} ~ 0.066 min^{-1}) is nearly two fold higher in comparison to CZTS (k_{app} ~ 0.032 min^{-1}). Various scavenger tests have been performed to establish the role of $O_2^{\bullet-}$ and •OH scavengers in the photo-degradation of the pollutant.

Introduction

The growing energy and environmental demand has led intensive research thrust on developing highly efficient, stable and low cost solar absorber materials. One of the primary goals is to produce high calorific hydrogen fuel from the abundant water available on the planet and to degrade the industrial dyes, which are carcinogenic and cause unwanted mutations in marine life cycles.[1] An extensive effort for the development of novel combination of materials to replace traditional semiconductors such as TiO_2, [2,3] ZnO,[4,5] CdS[6] etc. are underway. Over the last few decades several sulphide-based polynary alloy semiconductors have been explored and they proved as ideal photo-absorbers because of their tunable electronic and optical properties.[7-9] Compared to binary materials, polynary alloy semiconductor nano-materials are able to produce new properties as they could inherent the properties from their parent binary materials.[10] For example, several Cu-chalcopyrite p-type semiconductors namely $Cu(In,Ga)Se_2$,[11] $CuGa_3S_5$,[12] $CuGa_3Se_5$,[13,14] $CuInS_2$,[15,17] $Cu(In,Ga)S_2$,[16] $(CuIn)_xZn_{2(1-x)}S_2$[17] $CuGaSe_2$,[18] owing to their high absorption coefficients, tunable band gap values (1.0–2.4 eV) and suitable band alignment for water reduction, are used for H_2 production from water. However, the scarcity and higher cost of In, Ga has led to the search of alternative photo-catalytic systems from earth abundant elements such as Copper, Zinc etc.[19] Cu_2ZnSnS_4 which is non-toxic and its constituents are available plentiful (Cu: 50 ppm, Zn: 75 ppm, Sn: 2.2 ppm, S: 260 ppm)[20] is of interest as Cu_2ZnSnS_4 (CZTS) has a near-optimum direct band gap energy of 1.4-1.6eV and a large absorption coefficient (>10^4 cm^{-1}). Being environment friendly and of natural abundance, CZTS is finding its place in replacing high-efficient materials e.g. $Cu(InGa)Se_2$. Although, more emphasis is on fabricating photovoltaic solar cell devices of CZTS, [21-24] yet its photo-catalytic activity for waste water treatment, [25] photo-electrochemical devices[26] and water oxidation for hydrogen generation are also being explored[27]. The photo-catalytic efficiency of semiconductor materials is further enhanced by coupling them with either noble metals e.g. Au, Pt, [25] which act as co-catalyst, or making composite with material having large specific surface area and good electrical conductivity, namely Graphene oxide.[28] MoS_2 being a layered material with a large surface area, [29] is of interest as an alternative co-catalyst to the high cost noble metals. MoS_2 has shown high efficiencies when coupled with TiO_2, CdS etc.[30-33] which are studied for their photo-catalytic and solar water oxidation activity. Owing to their outstanding properties, we have studied CZTS and MoS_2 as possible candidates to replace

noble and other expensive elements for their photo-catalytic activity using CZTS as a photo-catalyst with MoS_2 as a co-catalyst. The water oxidation efficiency of CZTS-MoS_2 was observed to be nearly 20% higher than CZTS owing to a lesser recombination rate of photo-generated electrons and holes as evident from the photo-luminescence quenching in the CZTS-MoS_2 composite. The photo-catalytic degradation of a representative dye viz. Rhodamine B (RhB) was studied for the photo-catalytic activity of CZTS-MoS_2 composite; which shows a higher activity compared to CZTS alone as evident from the apparent rate constant for CZTS-MoS_2, which is nearly double (0.066 min^{-1}) than that of CZTS (0.032 min^{-1}). Various scavenger tests established that hydroxyl radical ($^{\bullet}OH$) plays a major role as the reactive intermediate species participating in dye degradation.

Experimental

Synthesis of Cu_2ZnSnS_4-MoS_2 composite

All reagents were of analytical grade and used without further purification. The synthesis of Cu_2ZnSnS_4 (CZTS) was adopted from the reference.[20] In a typical procedure, copper(II) acetate monohydrate (0.04M, 0.119g) (Merck), zinc(II) nitrate hexahydrate (0.02M, 0.089g) (Himedia), and tin(II) chloride dihydrate (0.02M, 0.067g) (Rankem) were dissolved in 15ml of a solvent mixture of ethylenediamine (EN) (Merck) and deionized water (volume ratio 1:9), wherein EN acts as a chelating agent and stabilizer. 15ml of 0.16M (0.182g) solution of thiourea, $SC(NH_2)_2$ (Merck) was added drop-wise to the above solution. Precursors' solution was then transferred into a 50ml Teflon-lined stainless steel autoclave, sealed and heated at 180ºC for 24h. Liu *et al.* have proposed that this process involves, the reduction of Cu^{2+} ions to Cu^{+} and oxidation of Sn^{2+} ions to Sn^{4+} through the oxidation–reduction reactions.[20] After cooling, the powders were centrifuged, washed several times with deionized water and absolute ethanol and dried at 60ºC overnight.

MoS_2 catalysts were synthesized by a hydrothermal method[34] involving ammonium heptamolybdate (0.276g) (Sigma- Aldrich) and thiourea (0.36g) (Merck), dissolved in 30mL distilled water. A surfactant cetyltrimethylammonium bromide (CTAB, 0.036g) (Rankem), was added into the above solution. Resultant mixture was added to a 50ml Teflon-lined stainless steel autoclave and kept at 180ºC for 24h. After cooling, catalyst was separated, washed with distilled water and absolute ethanol several times to remove the residual water and water-soluble impurities. Finally, the resulting product was dried at 50°C for 8h.

For the preparation of CZTS-MoS_2 composite, 1wt.% of MoS_2 was added into the above precursor solution of CZTS and transferred to a Teflon lined stainless steel autoclave, sealed and heated at 180ºC for 24h. Resulting powder, after cooling, was washed with water and ethanol several times and dried at 60°C overnight.

Characterization

The crystal structure of as prepared samples were characterized by powder X-ray diffraction (XRD) measurements using SEIFERT 3003-TT XRD machine operated at 40kV/30mA, (excitation wavelength CuK_{α}) . The scan range was 10°-80° with a step size of 0.03°/sec. Morphology and the compositional homogeneity of the photo-catalysts were studied using a Zeiss Sigma field emission scanning electron microscope (FE-SEM) operating voltage of 1−5kV and energy dispersive x-ray spectroscopy (EDX) at an operating voltage of 20kV respectively. UV–Visible diffuse reflectance spectra (DRS) of the samples were recorded on a Jasco V-650 spectrophotometer with an integrating sphere of 150 mm in the range of 200 to 800 nm. The absorbance of the RhB solution was measured in Perkin Elmer Lamda 25 UV-Visible spectrometer. The transmission electron microscopy (TEM) analysis was carried out using a JEOL JEM 2100 microscope at 200kV operating voltage. BET surface area was analysed by nitrogen (N_2) adsorption at liquid N_2 temperature with a Beckman-Coulter SA 3100 nitrogen adsorption apparatus. All the samples were degassed at 150°C for 2h prior to the N_2 adsorption measurements.

Photo-catalytic dye degradation experiment

Photo-catalytic dye degradation experiments for CZTS and CZTS-MoS_2 composites were performed separately in an immersion well photochemical reactor. The double-walled immersion well permits water circulation and it houses a MVL2 125W low pressure mercury vapour lamp as the light source to initiate the photo-catalytic reaction (SI). In a typical photo-catalytic degradation experiment, 100mL of aqueous Rhodamine-B dye (RhB) (10^{-5}M) and 0.05g of the photo-catalyst sample were loaded into the reactor. The reaction mixture was stirred overnight in the dark at room temperature in order to achieve adsorption–desorption equilibrium among the photo-catalyst, dye, dissolved oxygen and atmospheric oxygen. During irradiation, the suspension was kept stirring in order to achieve a homogeneous solution. 2mL of the sample was collected from the photo-reactor every ten minutes up to one hour. UV-Vis absorption spectra of the collected samples were recorded over the range 200–800nm after removing the solid catalyst particles by centrifugation. The concentration of the aqueous RhB was determined from the absorbance value monitored at 552nm.

Detection of reactive intermediates

To determine the reactive intermediates involved in dye degradation, photo-catalytic measurements were performed in presence of scavengers in the same way as mentioned in the dye degradation experiments. In our experiments, ethylenediaminetetraaceticacid (EDTA, 1mM), $FeSO_4$ (1mM) were employed as hole (h+) and $^{\bullet}OH$ scavengers respectively. Nitrogen gas is purged to remove the dissolved oxygen, which can serve as a test for $O_2^{\bullet-}$ scavenger.[35-37]

Photo-catalytic water oxidation to evolve hydrogen

Photo-catalytic water oxidation experiment to estimate hydrogen evolution, for CZTS and CZTS-MoS_2 were performed separately in a 100mL borosilicate round-bottom flask sealed with a silicone rubber septum, placed in a vessel containing a water inlet and an outlet to maintain the temperature of photo-reactor. The photo-catalytic reaction was carried out at room temperature and atmospheric pressure. A 500W tungsten halogen lamp (Halonix, India) was used as a light source to initiate the photo-catalytic reaction. The photo-catalyst sample was placed 15cm away from the lamp. In a typical photo-catalytic experiment, 0.2 g of sample was dispersed in 25mL of water containing Na_2SO_3 ($0.25molL^{-1}$) and Na_2S ($0.35molL^{-1}$) as sacrificial reagents. Solution containing the photo-catalyst was degassed for 30min and irradiated with UV–Vis light while stirring, to ensure uniform exposure of the suspension throughout the process. The produced gas was analysed by gas chromatography (Nucon 5765), using a thermal conductivity detector (TCD), after passing through moisture and oxygen traps (SI). In the absence of either light or the photo-catalyst, no appreciable amount of hydrogen was detected, suggesting that CZTS and CZTS-MoS_2 acted as the photo-catalysts in hydrogen production.

The apparent quantum yield (AQY) of the photo-catalyst was measured under the same reaction condition and it was calculated using the following equation: [38]

$$AQY = \frac{\text{Number of reacted electrons}}{\text{Number of incident photons}} \times 100\%$$

$$= \frac{2 \times \text{Number of hydrogen molecules evolved in 1 hour}}{\text{Number of incident photons in 1 hour}} \times 100\%$$

Results and discussion

Powder X-ray diffraction

The powder X-ray diffraction patterns of as-prepared CZTS, MoS_2 and the composite CZTS-MoS_2 are shown in Figure 1.

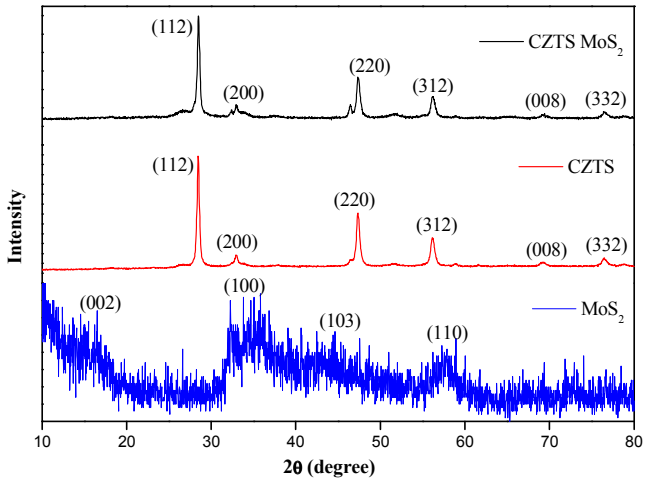

Figure 1: Powder X-ray diffraction patterns of Cu_2ZnSnS_4, MoS_2 and Cu_2ZnSnS_4-MoS_2 composite. Cu_2ZnSnS_4 and the composite show tetragonal kesterite structure whereas MoS_2 shows diffraction pattern corresponding to hexagonal structure

As-prepared CZTS was found to be crystallizing in tetragonal kesterite phase (JCPDS card no. 26-0575) as identified by reflections at $2\theta = 28.5^o$ (112), 33.3^o (200), 47.4^o (220), 56.1^o (312), 69.2^o (008) and 76.5^o (332). No impurity peaks corresponding to ZnS or Cu_2SnS_3 phases were observed as evident from Raman spectra (SI). Average crystallite size was calculated using Debye-Scherrer equation from the full width at half maximum (FWHM) of the reflection peak (112) and found to be ~4 nm for CZTS and 3.72 nm for CZTS-MoS_2 composite. There is no significant change observed in the crystallite size which is attributed to the interaction and adhering of CZTS to the surface of MoS_2 sheets.[39]

The as-prepared MoS_2 was weakly crystalline, as seen from the broadening of diffraction peaks. The PXRD pattern matched well with the hexagonal structure (JCPDS card no. 37-1592) with reflections at $2\theta = 16.7^o$, 33.4^o, 43.5^o and 57.4^o corresponding to (002), (100), (103) and (110) hkl planes respectively.

The composite CZTS-MoS_2 showed the XRD pattern of CZTS only, while no distinct peak corresponding to MoS_2 was observed. The absence of MoS_2 peaks could be attributed to the weak crystalline nature of MoS_2 compared to CZTS as well as the low content of MoS_2 i.e.~1% in the CZTS-MoS_2 composite. However, presence of MoS_2 has been established using the microscopic techniques such as EDX and TEM.

Morphological studies

Field Emission Scanning Electron Microscopy and Transmission Electron Microscopy

The morphological features of CZTS and its composite with MoS_2 are studied by field emission scanning electron microscopy and shown in Figure 2 (2A and 2B corresponds to CZTS and 2C, 2D are of CZTS- MoS_2).

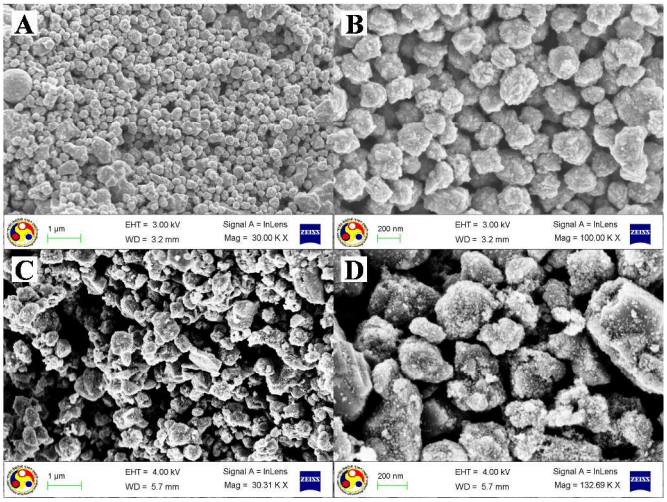

Figure 2: Field Emission scanning electron microscopic features; 2A and 2B show nearly spherical and similar size particle distribution of Cu_2ZnSnS_4, 2C and 2D show more aggregated particles of Cu_2ZnSnS_4-MoS_2

As-prepared CZTS showed nearly spherical particles of same size as seen in Figure 2A and 2B. The average particle size was observed to be in the range of ~200 nm, whereas, the composite showed bigger particles of irregular shape probably due to more CZTS particles getting accumulated into the MoS_2 layers. To ascertain the distribution of MoS_2, the elemental mapping of composite was recorded by energy dispersive X-ray analysis and observed that Molybdenum and Sulphur were homogeneously distributed throughout the sample as seen in Figure 3(A-F).

The interaction of CZTS and MoS_2 was further evaluated by transmission electron microscopy as shown in Figure 4. Figure 4A shows a nearly spherical composite particle and inset to Figure 4A shows the SAED pattern of CZTS-MoS_2 corresponding to tetragonal phase. Figure 4B and 4C shows the high resolution TEM image wherein a lattice spacing of 0.61nm corresponding to MoS_2 (100) plane and inter-planar distance of 0.32nm of CZTS (112) plane have been observed. This observation substantiates successful impregnation of MoS_2 on CZTS.

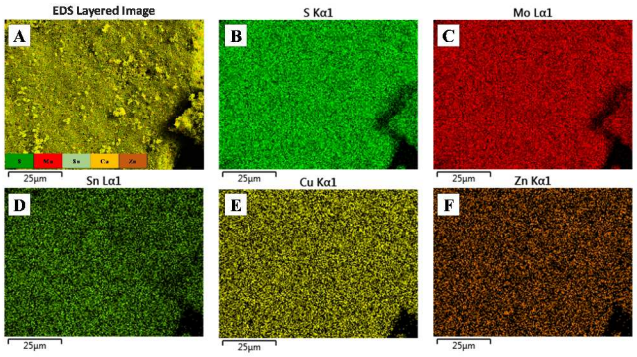

Figure 3 shows the compositional distribution of (A) Cu_2ZnSnS_4 - MoS_2 and the corresponding EDX elemental mapping of (B) S, (C) Mo, (D) Cu, (E) Zn and (F) Sn in the scan area of Figure 3 (A). The elemental mapping shows a homogeneous distribution of all the elements throughout the sample area.

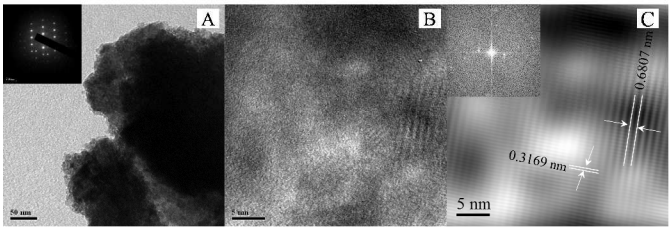

Figure 4: (A) shows the TEM image of Cu_2ZnSnS_4-MoS_2 and its SAED pattern is shown in the inset of (A). (B) High resolution transmission electron microscopy (HRTEM) image of Cu_2ZnSnS_4-MoS_2 (C) HRTEM showing lattice patterns of Cu_2ZnSnS_4 and MoS_2. Inset of (C) shows the FFT of the HRTEM image.

UV-Vis Diffuse Reflectance spectra

UV-Vis absorbance spectra of as-prepared CZTS, MoS_2 and their composite is shown in Figure 5 wherein all the samples show a broad absorption feature in UV, visible range. Inset to Figure 5 shows Tauc's plot to calculate the optical band gap of the material. The Tauc's equation is described as

$$(\alpha h\nu)^{1/n} = C \times (h\nu - E_g)$$

Where α is the absorption coefficient of the semiconductor at a certain value of wavelength λ, h is the Plank's constant, C is the proportionality constant, ν is the frequency of light, E_g is the band gap energy and n = ½ for direct transition mode materials respectively. The absorption coefficient is estimated from the equation,

$$\alpha = 1/t \times \ln (I_t/I_0) = 1/t \times A \times \log e$$

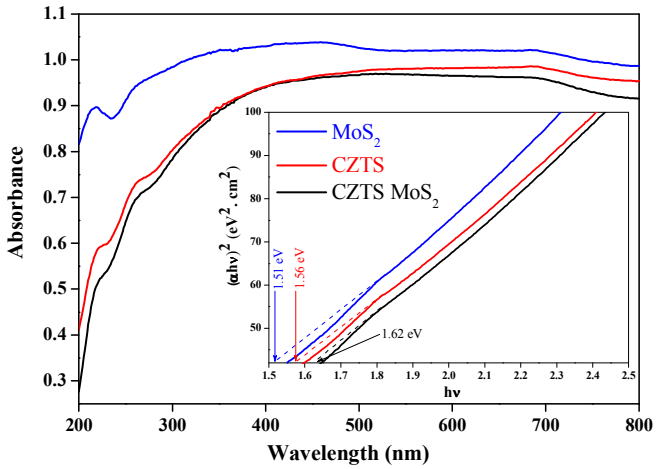

Figure 5 shows UV-Vis spectra of Cu_2ZnSnS_4, MoS_2 and Cu_2ZnSnS_4-MoS_2 depicting a broad absorption from UV and Visible range of the spectrum. The inset shows the Tauc's plot to evaluate the optical band gap values for the three compounds.

Where A, t, I_t and I_0 represent the absorbance, thickness of the photo-catalyst, intensity of transmitted light and intensity of incident light respectively. Tauc's plot shown in the inset to Figure 5 is plotted between $(\alpha h\nu)^2$ (on y-axis) and photon energy (hν) (on x-axis). The band gap energies were estimated by extrapolating lines and the band gap values for CZTS, MoS_2 and CZTS-MoS_2 are 1.56 eV, 1.51 eV and 1.62 eV respectively.

BET surface area analysis

Figure 6 shows N_2 adsorption-desorption isotherm and corresponding pore size distribution curve (inset) for CZTS and CZTS-MoS_2. According to the Brunauer-Deming-Deming-Teller (BDDT) classification, the majority of physisorption isotherms can be grouped into six types. The shapes of hysteresis loops are often used to identify the specific pore structure.[26] Both the samples display a typical type-IV isotherms and type H3 hysteresis loops. Type IV isotherms are generally shown by mesoporous industrial adsorbents.[40] The observed BET surface area of CZTS and CZTS-MoS_2 are 20.10 m^2/g and 17.17 m^2/g respectively. The Barrett–Joyner–Halenda (BJH) pore size distribution curve (inset) indicates the high degree of uniformity of pores in the range of ~3 nm for CZTS and ~7 nm for CZTS-MoS_2. Although the surface area for both samples are comparable, yet larger pore diameter in CZTS-MoS_2 suggests more effective active sites leading to enhanced photo-catalytic efficiency.

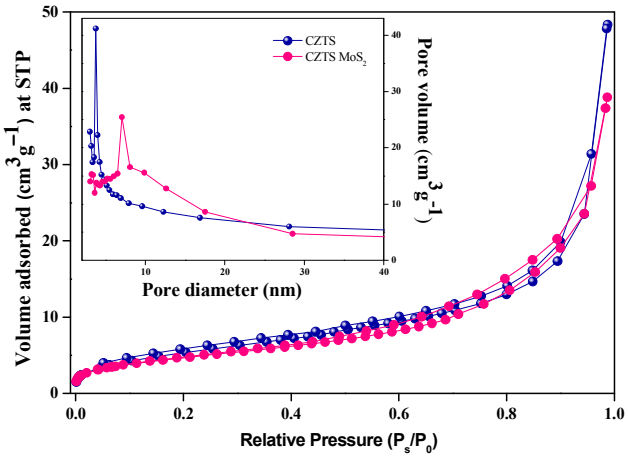

Figure 6 shows the BET surface area analysis of Cu_2ZnSnS_4 and Cu_2ZnSnS_4-MoS_2. Inset depicts Barrett–Joyner–Halenda pore size distribution curves for both the samples.

Photo-catalytic water oxidation

Photo-catalytic water oxidation experiment was carried out using CZTS and CZTS-MoS_2 as the photo-catalyst and the amount of hydrogen liberated were estimated using standard procedure. The H_2 evolution rates under visible irradiation are shown in Figure 7. The CZTS-MoS_2 composite showed a greater photo-catalytic activity with the H_2 production rate of 264 µmol/0.2g/h in comparison to bare CZTS (214 µmol/0.2g/h). The calculated AQY of CZTS-MoS_2 is 22.67% which is about 1.23 times higher than that of CZTS i.e. 18.42%.

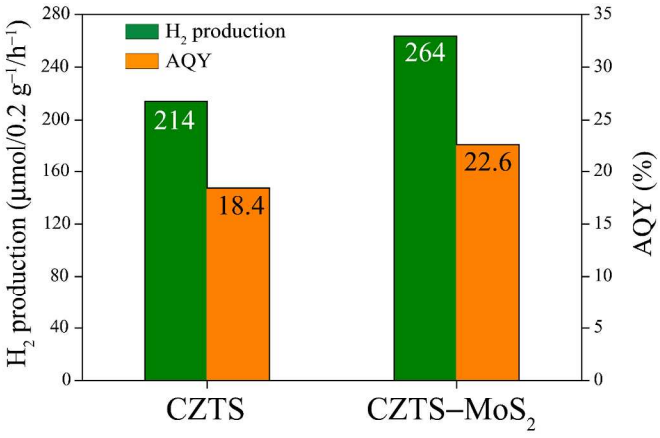

Figure 7: Amount of H_2 generated from Cu_2ZnSnS_4 and Cu_2ZnSnS_4-MoS_2 catalyst under light irradiation and their respective AQY (%) values.

The higher photo-catalytic activity is attributed to more active sites in CZTS-MoS_2 as well as higher charge separation. A schematic of the band diagram showing energy alignments of CZTS-MoS_2 which facilitates an efficient transfer of electrons is shown in Scheme 1. Upon light irradiation on CZTS-MoS_2, electron-hole pair is generated in CZTS in the CB and VB respectively. The sacrificial electron donor (Na_2SO_3) rapidly consumes the oxidative holes in the VB of CZTS, leaving the reductive electrons efficiently separated in the CB. At the same time, the reductive electrons are transferred from the CB of CZTS to the CB of MoS_2 because of the close proximity alignment of the conduction bands of the two, thereby leading to the reduction in the rate of electron–hole pair recombination hence enhanced charge separation. The pool of reductive electrons thus generated in the CB of MoS_2 promotes the reduction of H^+ ions, thereby producing H_2 gas. Thus, improved photo-catalytic activity of CZTS-MoS_2 is attributed to the efficient separation and lesser recombination of photo-generated electron–hole pairs in the composite.

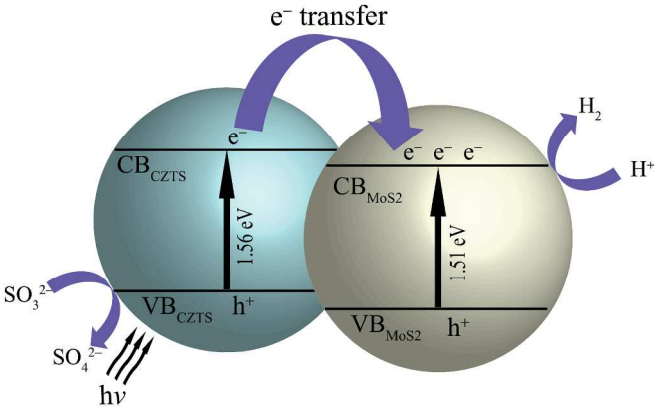

Scheme 1 Schematic representation of electron transfer of Cu_2ZnSnS_4 and MoS_2 in the composite.

The decrease in the recombination rate of electrons and holes in the composite is further substantiated by the quenching of fluorescence intensity (~ 11%) in the MoS_2 loaded CZTS compared to bare CZTS as seen in Figure 8.

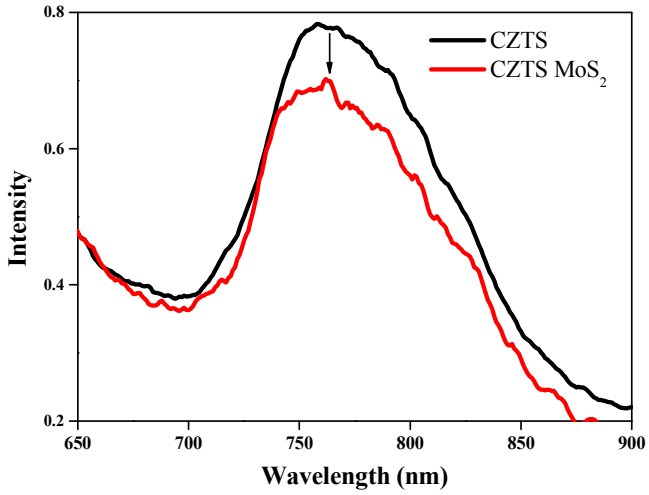

Figure 8 shows the photoluminescence spectra of Cu_2ZnSnS_4 and Cu_2ZnSnS_4-MoS_2. Emission intensity is quenched in case of the composite suggesting favourable charge separation of photo-generated electrons and holes

Reusability of CZTS-MoS_2

To examine the reusability of the CZTS-MoS_2 catalyst, we have carried out three cycles of the photocatalytic experiment of hydrogen production, with the catalyst. The catalyst retained optimal activity till three cycles, which shows the efficient reusability of the catalyst. The result of the repeated cycles is shown in Figure 9. In a typical experiment 0.2 g of sample was dispersed in 25mL of water containing Na_2SO_3 (0.25molL-1) and Na_2S (0.35molL-1) as sacrificial reagents. Solution containing the photo-catalyst was degassed for 30min and irradiated with UV–Vis light while stirring, to ensure uniform exposure of the suspension throughout the process. The produced gas was analysed by gas chromatography (Nucon 5765), using a thermal conductivity detector (TCD), after passing through moisture and oxygen traps. After irradiation of one hour, the solution was removed and the same experiment was repeated with fresh solution without any processing of the catalyst and the amount of gas evolved per 10 minutes was measured. Similarly, the experiment was repeated for a third cycle.

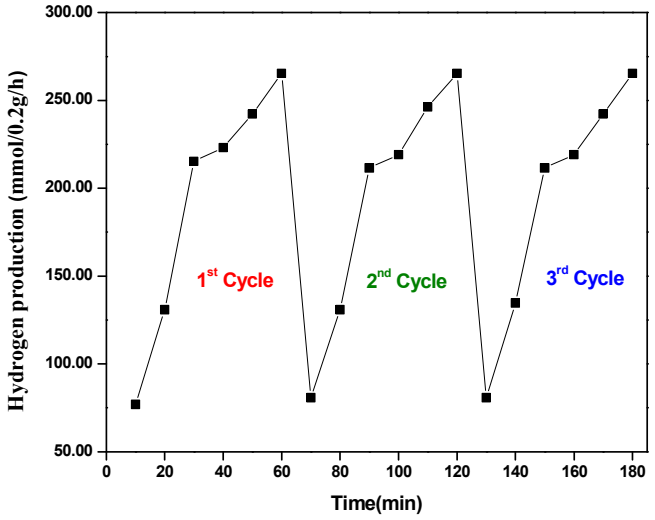

Figure 9: Amount of H2 generated from Cu2ZnSnS4-MoS2 catalyst after repeated cycles.

Photo-catalytic dye degradation analysis

The photo-catalytic dye degradation experiments were performed by suspending 0.05 gm of catalyst in a 100ml solution of Rhodamine B (RhB) (10^{-5}M) as a reference dye. The solution was stirred overnight in dark to achieve an adsorption-desorption equilibrium followed by an irradiation to start photo-catalytic dye degradation. The photo-degradation of RhB was followed by measuring its concentration at absorbance value of 552 nm. The absorbance spectra of RhB was collected at a regular intervals (10 min up to 1 hour) of degradation experiments, as shown in Figure 10a (catalyst used is CZTS) and Figure 10b (catalyst used is CZTS-MoS_2). The concentration (C/C_0) versus time is plotted as shown in Figure 11. From Figure 10, it is clearly observed that RhB was degraded much faster by CZTS-MoS_2 than CZTS alone. ~ 97% degradation of RhB was achieved in case of CZTS-MoS_2 in about 40 minutes whereas it was only ~70% for bare CZTS.

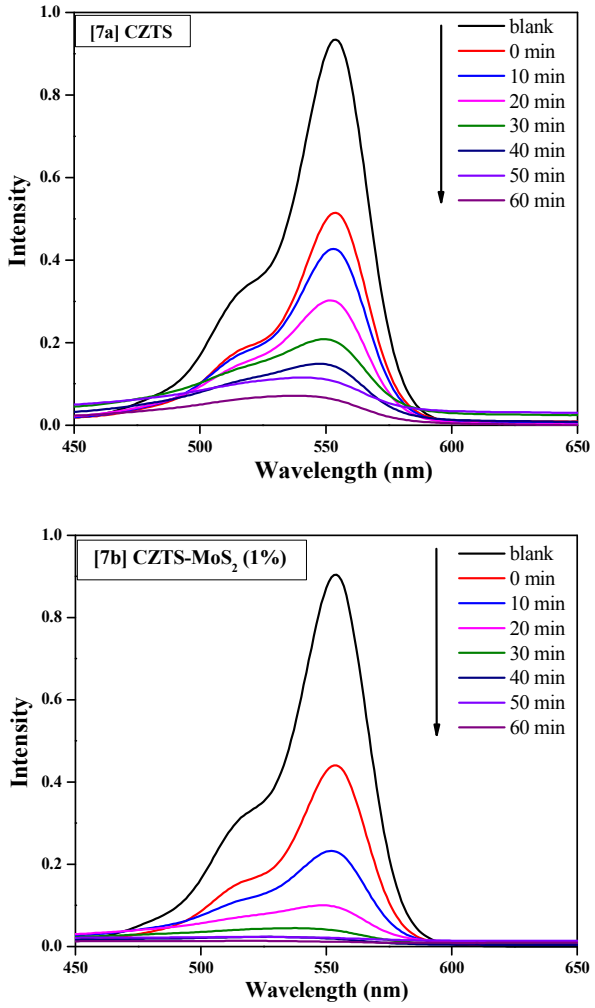

Figure 10(a) shows the UV-Vis absorption spectra of RhB degradation with Cu_2ZnSnS_4 catalyst; Figure 10(b) shows the UV-Vis absorption spectra of RhB degradation with Cu_2ZnSnS_4-MoS_2 catalyst

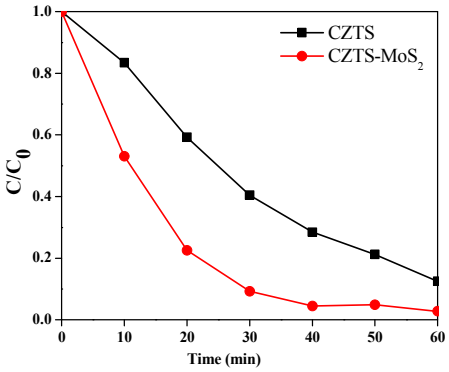

Figure 11 shows the C/C_0 versus irradiation time curves of photo-degradation of RhB by Cu_2ZnSnS_4 and Cu_2ZnSnS_4-MoS_2. The degradation is much faster in case of Cu_2ZnSnS_4-MoS_2.

Figure 12 shows the first order linear transform $\ln(C/C_0) = -k_{app}t$ corresponding to the photo-degradation of RhB by CZTS. Here, k_{app} is the apparent first order reaction rate constant which represents the rate of the reaction. CZTS-MoS_2 composite shows higher activity compared to CZTS alone as the apparent rate constant for CZTS-MoS_2 is almost twice (0.066 min^{-1}) than that of CZTS (0.032 min^{-1}).

Photo-catalytic dye degradation mechanism:

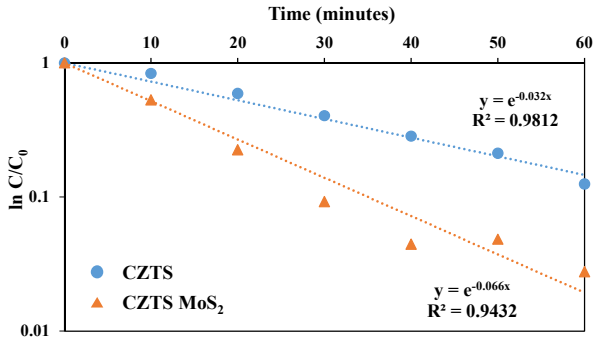

Figure 12 shows the evolution of apparent rate constant in the presence of Cu_2ZnSnS_4 and Cu_2ZnSnS_4-MoS_2

The photo-catalytic degradation of a dye generally takes place by the following mechanism.[35, 36] When a catalyst is exposed to UV-Vis irradiation, electrons are promoted from the valence band to the conduction band producing an electron–hole pair. The e^- and h^+ can migrate to the catalyst surface, where they can undergo a redox reaction with other species present on the surface. This prevents the recombination of the e^- and h^+ generated in the first step. h^+ (vb) can react easily with surface bound H_2O to produce $^{\bullet}OH$ radicals, whereas, e^- (cb) can react with O_2 to produce superoxide radical anion of oxygen, $O_2^{\bullet-}$. $^{\bullet}OH$ radicals can combine to form H_2O_2. The H_2O_2 can further react with $O_2^{\bullet-}$ to produce $^{\bullet}OH$, which is responsible for the degradation of the organic dye.

Catalyst + hυ → e^-_{cb} + h^+_{vb} Step 1

$e^-_{cb} + O_2 \rightarrow O_2^{\bullet-}$ Step 2

$h^+_{vb} + H_2O \rightarrow {}^{\bullet}OH + H^+$ Step 3

$^{\bullet}OH + {}^{\bullet}OH \rightarrow H_2O_2$ Step 4

$H_2O_2 + O_2^{\bullet-} \rightarrow {}^{\bullet}OH + OH^- + O_2$ Step 5

Dye + $^{\bullet}OH \rightarrow CO_2 + H_2O$ Step 6

It is seen that hydroxyl radical ($^{\bullet}OH$) and superoxide anion radical ($O_2^{\bullet-}$) are mainly responsible for the degradation of the dye. Therefore in order to study the mechanism of dye degradation, various scavenger tests were performed wherein radical or hole trapping agents were added into the dye catalyst system and the rate of degradation was observed.

Fe^{2+} salt was used as a $^{\bullet}OH$ trapping agent. Fe^{2+} undergoes the following reaction with $^{\bullet}OH$ present in the solution.

$\bullet OH + Fe^{2+} \rightarrow OH^- + Fe^{3+}$

This reaction has a very high rate constant ($k = 3.5 \times 10^8$ $M^{-1}s^{-1}$). In the presence of Fe^{2+}, $^{\bullet}OH$ is converted to OH^-, decreasing the $^{\bullet}OH$ concentration in the solution, leading to a decreased rate of dye degradation. SO_4^{2-} ions also causes a decrease in percentage degradation as they react with $^{\bullet}OH$ as-

$SO_4^{2-} + {}^{\bullet}OH \rightarrow SO_4^{2-} + OH^-$

Specificity of choosing $FeSO_4$ over other iron salts is that both cation and anion (Fe^{2+} and SO_4^{2-}) can act as the $^{\bullet}OH$ scavengers. The apparent rate constant (k_{app}) for RhB degradation in presence of $FeSO_4$ was less (0.004 min^{-1}) than that without the metal ion as can be seen in figure 14A.

Another important intermediate that plays an important role in the degradation process is superoxide radical anion ($O_2^{\bullet-}$) which is formed by the reduction of dissolved molecular oxygen in water. In order to prove its role, degradation experiment was carried out under continuous N_2 purging which is used to replace the dissolved oxygen from the system. The apparent rate constant (k_{app}) for degradation in deoxygenated water was less (0.025 min^{-1}) than that in normal oxygenated water (0.066 min^{-1}) as can be seen in figure 14B, proving the importance of dissolved oxygen in generating superoxide radical, which enhances the kinetics of degradation.

Further a degradation experiment was performed in the presence of EDTA which acts as a hole scavenger. The plot for apparent rate constant (k_{app}) for degradation showed a lower rate constant (0.012 min^{-1})in presence of EDTA as compared to the rate constant in the absence of EDTA (0.066 min-1) (Figure 14C)

Although, each scavenger has its role to play in controlling the kinetics of dye degradation, it was observed that $^{\bullet}OH$ plays more prominent role, evident from the kinetic data. Hence we propose that hydroxyl radical could be the determining species in controlling the kinetics of the dye degradation.

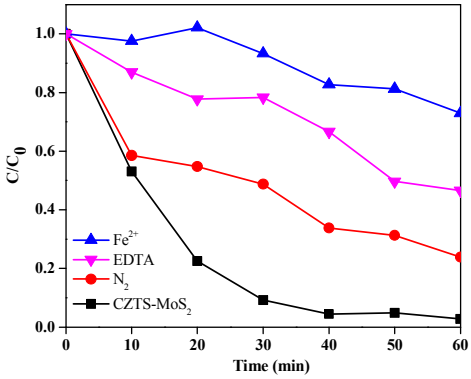

Figure 13 shows the concentration versus time for RhB degradation when different hole or hydroxyl radical scavengers were added along with the catalyst, suggesting that $^{\bullet}OH$ is the main intermediate reactive species promoting the dye degradation, as degradation is much slower in the presence of $FeSO_4$ (the hydroxyl radical scavenger).

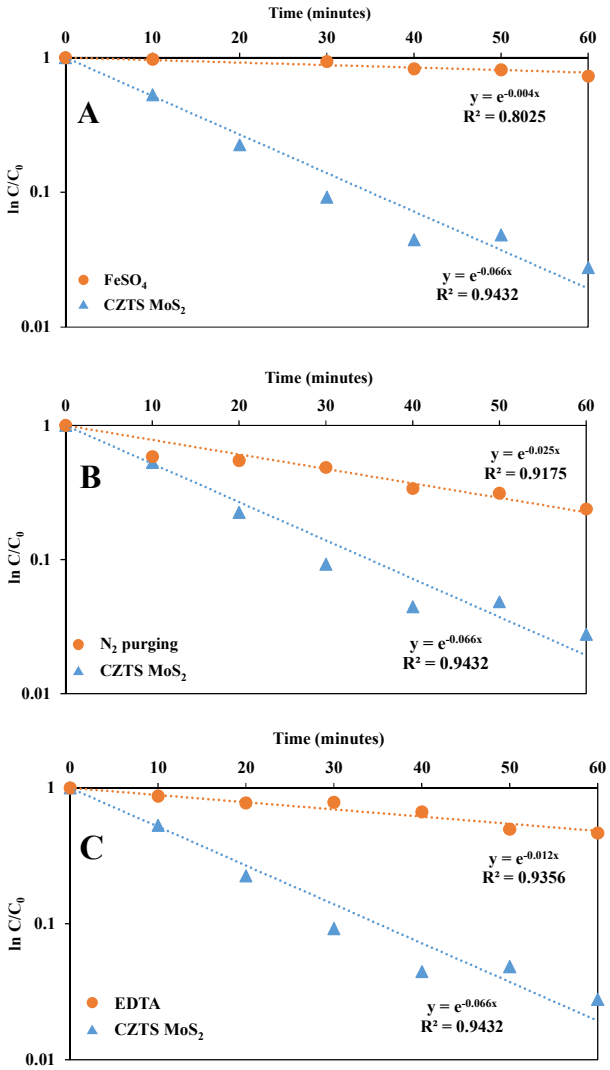

Figure 14A shows the evolution of apparent rate constant in the presence of Cu_2ZnSnS_4-MoS_2 and hydroxyl radical scavenger Fe^{2+}. The apparent rate constant of dye degradation in presence of Fe^{2+} (0.004 min^{-1}) is less than that in normal water containing the catalyst. Figure 14B shows the evolution of apparent rate constant in the presence of Cu_2ZnSnS_4-MoS_2 and superoxide radical anion scavenger, N_2. The apparent rate constant of dye degradation in presence of N_2 (0.025 min^{-1}) is less than that in normal water containing the catalyst. Figure 14C shows the evolution of apparent rate constant in the presence of Cu_2ZnSnS_4-MoS_2 and hole scavenger, EDTA. The apparent rate constant of dye degradation in presence of EDTA (0.012 min^{-1}) is less than that in normal water containing the catalyst.

Conclusion

In conclusion, quaternary Cu_2ZnSnS_4 and its composite with a layered material viz. MoS_2 were prepared by a facile hydrothermal method. The enhanced photo-catalytic ability of the composite was evaluated by its appreciable water splitting ability to evolve hydrogen with AQY value of 22.67%, and better efficiency in degradation of RhB as a reference pollutant, compared to bare CZTS. The faster photo degradation of RhB by CZTS-MoS_2 in comparison to CZTS is substantiated by kinetic studies. The various scavenger tests showed the major role of hydroxyl radical in the photo degradation of RhB.

Acknowledgements

MQ thanks CSIR Grant No: CSIR/01 (2704)/12/ EMR-II India for financial grant. SA thanks DST India for Women Scientist fellowship (WOS-A) Grant No: SR/WOS – A/CS-33/ 2013 (G): C/503/IFD/2014-15. The infrastructure and instrumentation help from IIT Guwahati, CIF – IIT Guwahati are highly appreciated.

References

Notes and references

[a] Materials Science Laboratory, Department of Chemistry, Indian Institute of Technology Guwahati, India - 781039. *mq@iitg.ernet.in

[b] Department of Chemical Engineering, Indian Institute of Technology Guwahati, India - 781039

† Electronic Supplementary Information (ESI) available: [Details of the experimental setup for photo catalytic hydrogen generation, Dye degradation setup, power spectrum distribution for the 500W tungsten halogen lamp are given . See DOI: 10.1039/b000000x/

References

1. Z. X. Chang, W.H. Zhou, D. X. Kou, Z. J. Zhoua and S.X. Wu, *Chem. Commun.*, 2014, **50**, 12726.; A. O. Ibhadon, and P. Fitzpatrick, *Catalysts*, 2013, **3**, 189-218; W. Y. Teoh, J. A. Scott and R. Amal, *J. Phys. Chem. Lett.* 2012, **3**, 629−639
2. A. Fujishima and K. Honda, *Nature*, 1972, **37,** 238.
3. A. L. Linsebigler, G. Lu, J. T. Yates, Chem. Rev., 1995, **95**, 735.
4. W. C. Lee, Y. Fang, R. Kler, G. E. Canciani, T. C. Draper ,Z. T.Y. Al-Abdullah, S. M. Alfadul, C.C. Perry, H. He, Q. Chen, *Materials Chemistry and Physics*, 2015, **149-150,** 12.
5. X. Zhang, J. Qin, Y. Xue, P. Yu, B. Zhang, L. Wang, R. Liu, *Scientific Reports*, 2014, **4**, Article number: 4596.
6. Z. Khan, T. R. Chetia, A. K. Vardhaman, D. Barpuzary, C. V. Sastri and M. Qureshi, *RSC Advances*, 2012, **2**, 12122.
7. A. L. Linsebigler, G. Lu and J. T. Yates, Jr., Chem. Rev., 1995, 95, 735; A. Kudo and Y. Miseki, *Chem. Soc. Rev.*, 2009, **38**, 253.
8. A. Shavel, J. Arbiol and A. Cabot, *J. Am. Chem. Soc.*, 2010, **132**, 4514.
9. S. Yang, Q. Yue, F. Wua, N. Huo, Z. Chen, J. Yang , J. Li, *Journal of Alloys and Compounds* , 2014, **597,** 91.
10. P. Hu, S. S. Pramana, S. Cao, C. K. Ngaw, J. Lin, S. C. J. Loo and T. T. Y. Tan, *Adv. Mater.*, 2013, **25**, 2567.
11. Yokoyama, T. Minegishi, K. Maeda, M. Katayama, J. Kubota, A. Yamada, M. Konagai, K. Domen, *Electrochem. Commun.* , 2010, **12**, 851.
12. M. Tabata, K. Maeda, T. Ishihara, T. Minegishi, T. Takata and K. Domen, *J. Phys. Chem. C*, 2010, **114**, 11215.
13. J. Kim, T. Minegishi, J. Kobotaa and K. Domen, *Energy Environ. Sci.*, 2012, **5**, 6368.
14. H. Kumagai, T. Minegishi, Y. Moriya, J. Kubota and K. Domen, *J. Phys. Chem. C*, 2014, **118**, 16386.
15. Gunawan, W. Septina, S. Ikeda, T. Harada, T. Minegishi, K. Domen and M. Matsumuraa, *Chem. Commun.*, 2014, **50**, 8941.

16. S. Ikeda, M. Nonogaki, W. Septina, G. Gunawan, T. Haradaa and M. Matsumuraa, *Catal. Sci. Technol.*, 2013, **3**, 1849.
17. I. Tsuji , H. Kato , H. Kobayashi ,and A. Kudo, *J. Phys. Chem. B*, 2005, **109**, 7323.
18. M. Moriya , T. Minegishi , H. Kumagai , M. Katayama , J. Kubota and K. Domen, *J. Am. Chem. Soc.*, 2013, **135**, 3733.
19. J. Wang, P. Zhang, X. Song and L. Gao, *RSC Adv.*, 2014, **4**, 27805.
20. W. C. Liu, B. L. Guo, X. S. Wu, F. M. Zhang, C. L. Mak and K. H. Wong, *J. Mater. Chem. A*, 2013, **1**, 3182.
21. T.R. Knutson, P.J. Hanson, E.S. Aydil, R.L. Penn, *Chem. Commun.*, 2014, **50**, 5902.
22. J. W. Cho, A. Ismail, S. J. Park, W. Kim, S. Yoon and B. K. Min, *ACS Appl. Mater. Interfaces*, 2013, **5**, 416.
23. S. K. Saha, A. Guchhait and A. J. Pal, *Phys. Chem. Chem. Phys.*, 2012, **14**, 8090.
24. B. Shin, O. Gunawan, Y. Zhu, N. A. Bojarczuk, S. J. Chey, S. Guha, Prog. *Photovolt: Res. Appl*., 2013, **21**, 72.
25. X. Yu, A. Shavel, X. An, Z. Luo, M. Ibanez and A. Cabot, *J. Am. Chem. Soc.*, 2014, **136** , 9236.
26. S. C. Riha, S. J. Fredrick, J. B. Sambur, Y. Liu, A. L. Prieto and B. A. Parkinson, *ACS Appl. Mater. Interfaces*, 2011, **3**, 58.
27. E. Ha, L. Y. S. Lee, J. Wang, F. Li, K-Y Wong and S. C. E. Tsang, *Adv. Mater.*, 2014, **26**, 3496.
28. D. Chen, Y. Zhao, Y. Chen, B. Wang, H. Chen, J. Zhou and Z. Liang, *ACS Appl. Mater. Interfaces*, 2015, **7**, 3224−3230; L. Bai, J.N. Ding, N.Y. Yuan, H.W. Hu, Y. Li, X. Fang, *Materials Letters*, 2013, **112**, 219.
29. S. Yang, J. Kang, Q. Yue, and K. Yao*, J. Phys. Chem. C*, 2014, **118**, 9203.
30. T. Jia, A. Kolpin, C. Ma, R. C.T. Chan, W.M. Kwok and S. C. E. Tsang, *Chem. Commun.*, 2014, **50**, 1185.
31. Y.L. Min, G. Q. He, Q. J. Xu and Y. C. Chen, *J. Mater. Chem. A*, 2014, **2**, 2578.
32. M. Shen, Z. Yan, L. Yang, P. Du, J. Zhang and B. Xiang, *Chem. Commun*., 2014, **50**, 15447.
33. Y. Zhu, Q. Ling, Y. Liu, H. Wangb and Y. Zhu, *Phys. Chem. Chem. Phys.*, 2015, **17**, 933.
34. W. Wang, K. Zhang, Z. Qiao, L. Li, P. Liu and Y. Yang, *Ind. Eng. Chem. Res*., 2014, **53**, 10301.
35. Z. Khan, T. R. Chetia and M. Qureshi, *Nanoscale*, 2012, **4**, 3543.
36. M.A. Rauf, S. S. Ashraf, *Chemical Engineering Journal*, 2009, **151**, 10.
37. G. Naresh and T. K. Mandal, *ACS Appl. Mater. Interfaces*, 2014, **6**, 21000.
38. R. Sasikal, V. Sudarsan, C. Sudakar, R. Naik, T. Sakuntala and S. R. Bharadwaj*, J. Phys. Chem. C*, 2012, **116**, 150.
39. J. Li, K. Yu, Y. Tan, H. Fu, Q. Zhang, W. Cong, C. Song, H. Yin and Z. Zhu, *Dalton Trans.* 2014, **43**, 13136; Y.Zhu, Q. Ling, Y.Liu, H. Wangb and Y.Zhu, *Phys. Chem. Chem. Phys.* 2015, **17***,* 933.
40. K. S. W. Sing, D. H. Everett, R. A. W. Haul, L. Moscou, R. A. Pierotti, J. Rouquerol and T. Siemieniewska, *Pure & Appl. Chem.*, 1985, **57**, 603.

Graphical Abstract:

Quaternary semiconductor Cu_2ZnSnS_4 loaded with MoS_2 as co-catalyst for enhanced photo-catalytic activity

Gaurangi Gogoi[a], Sonia Arora[a], Natarajan Vinothkumar[b] ,Mahuya De[b]and Mohammad Qureshi*[a]